Elastic and inelastic scattering of 100 MeV protons from the even-even titanium isotopes

L. W. Woo,* N. S. Wall, P. G. Roos, P. H. Debenham,† K. Kwiatkowski,* and A. Nadasen‡
Department of Physics and Astronomy, University of Maryland, College Park, Maryland 20742
(Received 13 September 1983)

The differential cross sections for elastic and inelastic scattering to the first excited (2^+) states of 100 MeV protons from ^{46,48,50}Ti were measured. The angular ranges covered were 9° to 110° for ^{46,50}Ti and 9° to 168° for ^{48}Ti. The elastic scattering data were analyzed with a local optical model potential. The quality of fits to the data covering the smaller angular range ($<110°$) is good for all three isotopes, with $\chi^2/N \sim 1.5$; whereas the fit to the large angle data of ^{48}Ti ($\lesssim 168°$) is not as satisfactory ($\chi^2/N \sim 3.75$). Various modifications to the Woods-Saxon shape of the real central potential showed no real improvement. Nevertheless, the large angle data appear to favor a slightly sharper falloff in the real central potential near the surface, such as the Woods-Saxon-squared potential. Systematics of the phenomenological optical model potential of 100 MeV protons were studied. The derived volume integrals and rms radii seem to follow the usual A dependence. The isospin dependence of the real potential was also extracted. The mean free paths computed directly from the imaginary potential strength have large uncertainties due to the insensitivity of the data to the central region of the imaginary potential. Distorted-wave Born approximation and coupled-channels Born approximation calculations for the collective excitation of the target nuclei to the first 2^+ states provided deformation parameters, β_2, in agreement with those from other proton and alpha scattering data and electromagnetic measurements.

I. INTRODUCTION

The central feature of the optical model (OM) is the representation of the complicated interaction between a bombarding particle and a nucleus by a one-body complex potential, which is of short range, depends only on the relative spatial coordinate, and varies rather smoothly with the incident energy. Thus, the tremendously complicated description of the many-body projectile-target system is reduced to the solution of the Schrödinger equation with a single complex potential.

Since its introduction the OM has been employed very successfully in the analysis of extensive neutron and proton elastic scattering data. Feshbach, Porter, and Weisskopf[1] successfully used the one-body potential for neutrons impinging on a wide range of targets. The phenomenological work of Perey, and Perey and Buck[2] on the elastic scattering and polarization of protons of 9–22 MeV from several nuclei showed that the best fit form factor parameters are strikingly similar, suggesting that the elastic scattering to a large extent reflects the nuclear density distribution. Furthermore, they found that the depth of the real potential depends linearly on the incident energy and on the neutron excess or symmetry parameters, $(N-Z)/A$, of the target. These findings are not particularly surprising, since essentially all formal theories show the optical potential to be inherently nonlocal. A smooth energy dependence in the strength of a local potential arises rather naturally from a Fourier transform of a nonlocal potential to an equivalent local potential. Similarly, in any theoretical treatment of proton-nucleus collisions in an isospin formalism, the dependence on the symmetry parameter arises automatically from a $\vec{t}_p \cdot \vec{T}_t$ operator, where t_p and T_t are the proton and nucleus isospins, respectively. The early successes paved the way for global OM analyses of large sets of data by Becchetti and Greenlees,[3] Van Oers and others.[4] Generally, the OM seems to be a quite adequate description for nucleon-nucleus elastic scattering up to about 200 MeV,[5–8] as long as reasonable flexibility in the shape of the potential is allowed, for example, the use of sums of Woods-Saxon potentials.

Theoretical development in the OM has also enjoyed recent prominence. For example, the use of an effective nucleon-nucleon interaction in the calculation of the real part of the optical potential from the convolution of the nuclear density and the effective interaction (the folding model) has been investigated extensively.[9] Also, the relativistic formulation of the optical model potential (OMP) was studied quite exhaustively by Arnold *et al.*[10] More recently, advances have been made in the application of nuclear matter techniques to the calculation of the OMP with a realistic nucleon-nucleon interaction by Jeukenne, Lejeune, and Mahaux,[11] and Brieva and Rook.[12] The energy dependence of the strengths of the various components of the potential, the isospin dependence, and the shape and energy dependence of the form factor derived from these theoretical treatments can be tested by comparison with phenomenological analyses.

In spite of these theoretical advances and empirical successes we nevertheless still often encounter a great deal of uncertainty in the understanding of the nucleon-nucleus interaction. With this view in mind we decided to make extensive measurements of elastic scattering of 100 MeV protons from the even-even Ti nuclei. The aim of the project is to:

(1) Obtain OMP parameters for comparison with exist-

ing proton elastic scattering analyses at other energies.

(2) Make isotopic size comparisons among the even-even titanium isotopes and to compare our results with those of electron, alpha, and other proton scattering.

(3) Study the isospin dependence of the OMP for protons at 100 MeV.

(4) Investigate the validity of the OMP in its conventional form to describe large angle elastic scattering data.

(5) Evaluate the various distorted wave treatments of inelastic scattering data.

Brief descriptions of the experiment, data reduction, and error analysis are given in Sec. II, and the experimental results are given in Sec. III. In Sec. IV we discuss the OM analysis of our data, isotopic size comparison, and the systematics of the OMP. In Sec. V, we present analyses of the inelastic scattering data based on DWBA and the CCBA formalism. Finally, the results are summarized in Sec. VI.

II. EXPERIMENT

The experiment was carried out using a 101.3 MeV momentum analyzed proton beam from the University of Maryland Sectored Isochronous Cyclotron. The energy resolution of the beam was 0.04%, and the beam spot on target was typically 2.5 mm high by 1.5 mm wide.

The small angle ($\theta < 60°$) and large angle ($\theta > 100°$) measurements were made in a 1.5 m diam high precision scattering chamber, equipped with two remotely controlled arms. A stack of two 2.5 cm diam and 1.36 cm deep high purity Germanium crystals mounted on one arm were used for detecting protons. The system provided an energy resolution ranging from 130 to 250 keV. A 3.175 cm diam and 6.35 cm deep NaI(Tl) detector mounted on the other arm served as a beam monitor. The angular position of the arms could be measured to an accuracy of 0.02°.

The intermediate angles (50°—120°) were measured with a QDS magnetic spectrometer coupled to a 43 cm diam scattering chamber. The spectrometer consisted of an entrance quadrupole, a $n = \frac{1}{2}$ 180° dipole and an exit sextupole. A resistive wire proportional counter placed at the focal plane was used for position measurement. This was followed by two plastic scintillators which served as ΔE detectors for particle identification. The resolution obtained was ~ 100 keV.

The angular offset of the beam about the geometrical zero angle was determined by the crossover method using a CH target as well as by measuring elastic scattering cross sections of the Ti targets on both sides of the beam. The beam current was monitored with an internal Faraday cup in the spectrometer and an external Faraday cup for the large scattering chamber.

Signals from all detectors were fed into charge sensitive preamplifiers. The fast outputs from the preamplifiers were used for the fast coincidence and pileup rejection circuits in order to reduce background events. The slow signals after being suitably amplified and gated by the appropriate coincidence requirements were fed to 4096 channel ADC's interfaced to an IBM 360/44 computer. Proton energy spectra were generated for each measurement and stored on magnetic tapes. Electronic dead time was measured by generating pulses at a rate proportional to the beam current, feeding them to all preamplifiers and processing them together with the real data. The computer dead time was automatically corrected for by gating off the events and the current integrator with the busy signal from the interface unit.

Two sets of isotopically enriched ^{46,48,50}Ti targets were used. The thinner targets (~ 5 mg/cm^2) were used for the forward angle measurements while the thicker targets (~ 16 mg/cm^2) were used for the large angle data. At each angle data were accumulated until the elastic or first excited state (2^+) had $\lesssim 2\%$ statistics for $\theta \lesssim 60°$ and $\lesssim 10\%$ for $60° \lesssim \theta \lesssim 110°$. For $\theta > 110°$ the runs were limited to six hours per data point. To optimize on resolution, the target angle was usually maintained at half the detector angle. To check for systematic errors, data were taken in larger steps with increasing angle. Then the angles were decreased to fill in the intermediate points. Due to limitations of beam time, large angle data were obtained for only the ^{48}Ti target.

The magnetic tapes were later replayed and the areas under the elastic, 2^+, and pulser peaks were obtained. The error in peak extraction was generally 1%. Since ^{46,50}Ti target contained $\geq 10\%$ of ^{48}Ti contamination, isotopic corrections were made for the forward angle data where the various isotopes could not be separated. The relative error resulting from this procedure was estimated to be less than 1%.

The statistical uncertainties were ~ 1—2% for $\theta \lesssim 60°$, $\sim 5\%$ for $\theta \lesssim 90°$, and $\sim 10\%$ for $\theta \lesssim 110°$. Because of the low cross sections the errors were much larger ($\gtrsim 20\%$) for the large angle data.

The angle uncertainty in the detector setting ($\pm 0.02°$) and beam zero angle ($\pm 0.05°$) gave a total uncertainty of $\pm 0.07°$. The relative error due to this uncertainty depends on the rate of change of cross section with angle, and varied from zero to a few percent. The uncertainty in the dead time correction contributed less than 0.5% to the total relative error.

The uncertainty in the absolute normalization of the cross sections came mainly from measurements of solid angle (~ 1—3%), target thickness ($\sim 5\%$), integrated beam current ($\sim 1\%$), and correction for the reaction tail of Ge ($\sim 3\%$). Adding these in quadrature gives a total uncertainty in the normalization of the data of approximately 7%.

III. EXPERIMENTAL RESULTS

The differential cross sections for elastic scattering and the 2^+ state were measured over angular ranges of $9° \lesssim \theta_{\text{c.m.}} \lesssim 110°$ for ^{46,50}Ti and $9° \lesssim \theta_{\text{c.m.}} \lesssim 168°$ for ^{48}Ti. ^{48}Ti was chosen for the large angle data because of its high degree of isotopic purity. The results are shown in Figs. 1 and 2.

The general features of the angular distributions are as follows:

(1) From 9° to 110° for all three isotopes, σ_{el} changes from $\sim 10^3$ to $\sim 10^{-4}$ mb/sr and σ_{2^+} from $\sim 10^1$ to $\sim 10^{-4}$ mb/sr. The oscillatory patterns for σ_{el} and σ_{2^+}

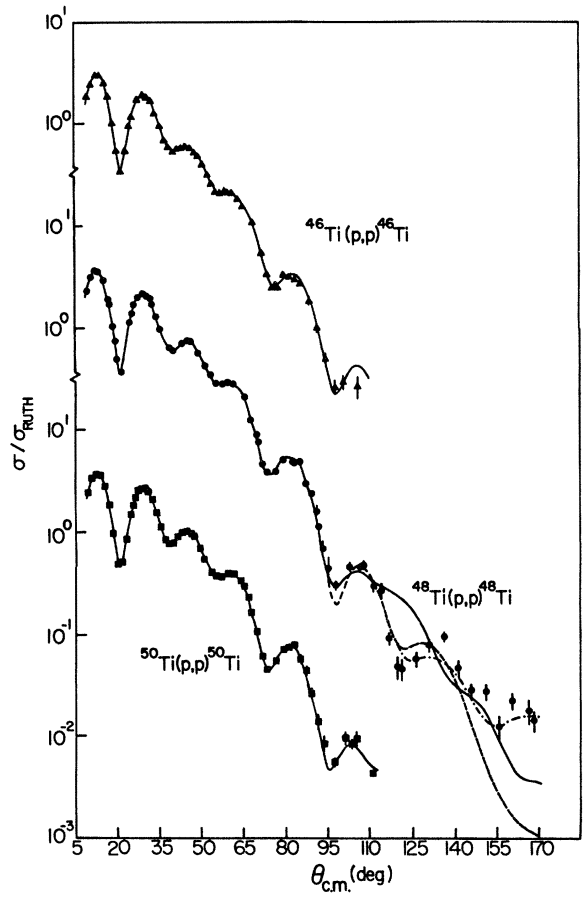

FIG. 1. 100 MeV p+^{46,48,50}Ti elastic differential cross sections plotted as ratio to Rutherford. The solid lines are optical model fits to the 9°—110° data using a WS form factor. The dashed line is obtained by fitting the 9°—168° data of ^{48}Ti. The dotted-dashed line is obtained with a WS^2 potential.

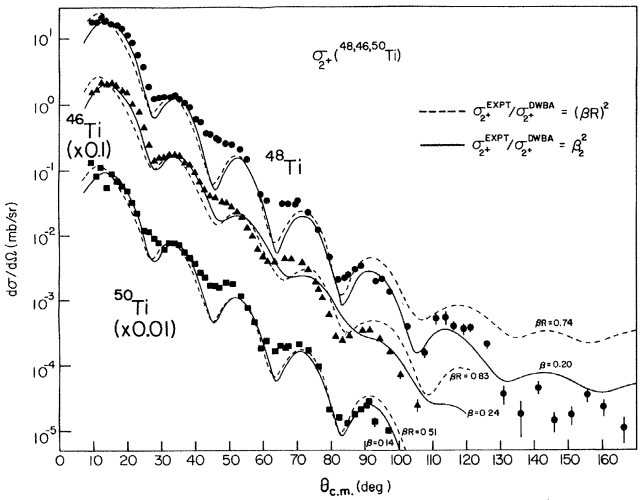

FIG. 2. Differential cross sections for the first 2$^+$ states in ^{48,46,50}Ti. Also shown are DWBA calculations which scale as $(\beta_2)^2$ (solid lines) and $(\beta_2 R)^2$ (dashed lines).

are quite similar and seem to follow the Blair phase rule. σ_{2+} becomes comparable to σ_{el} at $\sim 70°$ and falls more slowly with angle than σ_{el}. This behavior continues all the way to the backward angles. In the case of ^{48}Ti at $\theta \simeq 160°$ σ_{2+} is almost 2.5 times σ_{el}.

(2) After the first maximum, the oscillations become rather damped until $\theta_{c.m.} \simeq 70°$ beyond which the oscillations again become quite pronounced. The peak in σ_{el} near $\theta \sim 80°$ is most pronounced for ^{46,50}Ti and is relatively weak for ^{48}Ti. This is very likely due to some interference between the spin-orbit and the central potentials, since this region is most sensitive to the spin-orbit term.[6]

(3) For ^{48}Ti, beyond 110°, the slopes of both σ_{el} and σ_{2+} become less steep. In fact, σ_{el} lies completely within one decade for the next 60°. This less-steep slope of σ_{el} at backward angles is normally attributed to exchange effects. However, the introduction of a simple exchange term of the "Majorana-type" does not adequately reproduce the large angle data of ^{48}Ti.

(4) σ_{el} shows the usual dependence on the nuclear radius, $\sim r_0 A^{1/3}$, i.e., the first minimum shifts toward smaller θ as A increases.

(5) Finally, σ_{el} is largest for ^{50}Ti and smallest for ^{46}Ti, whereas the reverse trend is observed in σ_{2+}. This feature is also observed in the scattering of 140 MeV alpha particles from the same Ti isotopes.[13] This result is consistent with other experiments which indicate that in a collective model treatment the deformation (βR) of ^{46}Ti is largest and that of ^{50}Ti is smallest.

IV. OPTICAL MODEL ANALYSIS

The optical model analysis of the elastic scattering data was carried out with a modified version of the Oak Ridge optical model code JIB III. The nonrelativistic local Schrödinger equation was solved using the Cowell numerical method,[14] with an optical model potential consisting of complex central and spin-orbit terms and a Coulomb term:

$$-U_R f(r,r_R,a_R) - iW_V f(r,r_I,a_I) - (V_{so}+iW_{so}) \times \left[\frac{h}{m_\pi c}\right]^2 \frac{1}{r}\frac{d}{dr} f(r,r_{so},a_{so})\vec{l}\cdot\vec{\sigma} + U_C(r) ,$$

where $f(r,r_x,a_x)$ is the Woods-Saxon form

$$\left[1+\exp\left[\frac{r-r_x A^{1/3}}{a_x}\right]\right]^{-1}$$

and $U_C(r)$ is the Coulomb potential due to a uniform sphere of charge.

The code simultaneously searches on up to ten parameters, namely U_R, r_R, a_R, W_V, r_I, a_I, V_{so}, W_{so}, r_{so}, and a_{so}. The quantity to be minimized was defined as

$$\chi^2 = \sum_{i=1}^{N} \left[\frac{\sigma^{JIB}(\theta_i)-\sigma^{expt}(\theta_i)}{\Delta\sigma(\theta_i)}\right]^2 + \left[\frac{\sigma_R^{JIB}-\sigma_R^{expt}}{\Delta\sigma_R}\right]^2 ,$$

where N is the number of differential cross section data points, $\sigma(\theta_i)$ is the differential cross section, σ_R is the total reaction cross section, and $\Delta\sigma$ is the experimental er-

rors in the data. The value of 674 mb with an uncertainty of 3%, obtained experimentally by Kirky and Link,[15] was used for σ_R.

The "stability" of the numerical computation was determined by repeating "one-shot" calculations using different matching radii (R_m) and integration step sizes (h). R_m was varied from 10 to 20 fm, and h from 0.12 to 0.06 fm. In all the calculations, the maximum number of partial wave scattering amplitudes computed was ≤ 28. For $\theta \leq 110°$, $d\sigma/d\Omega$ remained essentially unchanged for values of R_m and h within the ranges stated. At larger angles, the calculated cross section $d\sigma/d\Omega$ seemed to reach a plateau, as a function of R_m and h, centered around $R_m \simeq 15$ fm and $h=0.08$ fm. Therefore, $R_m=10$ fm and $h=0.10$ fm were used in all calculations covering the angular range from 9° to 110° and $R_m=15$ fm and $h=0.08$ fm for the large angle data of ^{48}Ti.

A. OMP parameter search procedure

Since the data of ^{46,50}Ti covered only the angular range of 9° to 110°, while that of ^{48}Ti was from 9° to 168°, the analysis was divided into two parts: $9° \leq \theta \leq 110°$ for ^{46,48,50}Ti in order to make isotopic comparisons and $9° \leq \theta \leq 168°$ for ^{48}Ti.

The starting parameters for the OMP were those of 100 MeV p+^{58}Ni,[5] and full ten-parameter searches were carried out. Besides minimum χ^2, the "best fit parameters" were required to give reasonable values for the volume integrals of the real and imaginary central potentials (~ 260 and ~ 100 MeV fm^3, respectively) and to reproduce the experimental total reaction cross section, σ_R, to within two experimental standard deviations. The best-fit parameters are presented in Table I and the fits to the experimental data shown in Fig. 1 (solid lines).

The ^{46}Ti data gave results that were slightly different from expectations based on the work of Kwiatkowski and Wall[5] and Nadasen and co-workers:[6] the real volume integral J_R/A and the spin orbit strength U_{so} being somewhat smaller and the imaginary volume integral J_I/A larger. Attempts to obtain fits with more consistent parameters were unsuccessful.

B. Parameter sensitivity to change in absolute normalization

In view of the 7% uncertainty in the absolute normalization of the data, the effects of a change in normalization on the OMP parameters for all three sets of data were investigated. The dependence of the chi-square per data point, χ^2/N, on the normalization was relatively weak and almost parabolic, with the minimum centered around -4% change in normalization.

The parameters of the real central potential varied monotonically with change in normalization. The potential strength, U_R, changed by about $+0.2$ MeV, the radius parameters, r_R, by about -0.003 to -0.001 fm, and the volume integral, J_R/A, by about $+1.5$ MeV fm^3 per 1% change in normalization. The imaginary central potential parameters, W_V, r_I, and a_I, exhibited a rather unexpected dependence on the normalization change. All three parameters reached either a maximum or minimum

TABLE I. Best fit parameters.

Target nucleus	U_R	r_R	a_R	W_V	r_I	a_I	U_{so}	W_{so}	r_{so}	a_{so}	J_R/A	$\langle R^2\rangle_R^{1/2}$	J_I/A	$\langle R^2\rangle_I^{1/2}$	σ_R[c]	χ^2/N
^{46}Ti[a]	20.64	1.306	0.715	14.27	1.212	0.632	0.732	−2.44	1.021	0.481	237.0	4.795	128.7	4.103	633	1.57
^{48}Ti[a]	24.35	1.255	0.784	9.38	1.392	0.553	2.26	−2.21	1.049	0.478	260.4	4.580	118.5	4.425	696	1.39
^{50}Ti[a]	23.82	1.278	0.739	9.78	1.378	0.522	2.16	−2.66	1.037	0.458	258.9	4.566	118.4	4.385	701	1.67
^{48}Ti[b]	23.81	1.268	0.744	10.13	1.328	0.665	1.69	−2.47	1.035	0.485	255.6	4.516	118.0	4.482	699	3.75
Exchange[b]	23.86	1.267	0.745	10.22	1.326	0.664	1.70	−2.48	1.034	0.484	255.7	4.514	118.5	4.475	700	3.25
Wine bottle[b]	24.06	1.266	0.748	10.19	1.330	0.661	1.61	−2.54	1.037	0.485	247.5	4.276	119.0	4.478	700	3.22
WS[2b]	23.95	1.499	0.857	7.65	1.457	0.554	2.77	2.05	1.063	0.535	263.7	4.655	109.8	4.590	686	3.17

[a]Parameters from $9° \leq \theta \leq 110°$ fit.
[b]Parameters from $9° \leq \theta \leq 168°$ fit.
[c]σ_R obtained from otpical model analysis.

at about -5% normalization.

The spin-orbit potential parameters and, as a result, the predicted polarizations, were also very sensitive to changes in absolute normalization. Even though the quality of fit to the elastic cross section remained virtually unaffected, the polarization changed significantly. This fact was also observed by Ingermarsson and Tibell at 180 MeV.[16] This, of course, stresses the importance of having both polarization and differential cross section data in OM analyses. It must be noted that the calculated polarization of ^{46}Ti is quite different from those of ^{48}Ti and ^{50}Ti. This seems to be a reflection of the rather small real spin-orbit strength of ^{46}Ti.

C. Analysis of the large angle data of ^{48}Ti: $9° \leq \theta_{c.m.} \leq 168°$

1. Fit with Woods-Saxon potential

The fit to the large angle data of ^{48}Ti was initiated by starting with the best-fit Woods-Saxon parameters obtained for smaller angular range data. There was no significant change in the parameters except for a reduction in the spin-orbit strength U_{so}. The resulting parameters are also listed in Table I. A comparison of the two fits is shown in Fig. 1. The two calculations are visually indistinguishable from each other at more forward angles, and little improvement is obtained for the large angle data.

The simple Woods-Saxon potentials predict that the elastic cross section would continue to fall with about the same average slope all the way out to 180°, whereas the data fall at a slower rate for $\theta_{c.m.} > 130°$.

2. Exchange effect

It has been shown[17] that the antisymmetrization of the nucleon-target system can be approximated by an effective OMP consisting of both direct and exchange terms. Greenlees *et al.*[18] have studied the exchange potential resulting from the "target exchange" or "heavy particle pickup" in the elastic scattering of 30 MeV protons from ^{40}Ca, and showed clearly that such a term strongly affects the elastic scattering cross section and the polarization at angles greater than 100°. Also, the OM analysis of p+^{4}He elastic scattering at various energies[19] showed unambiguously the importance of a Majorana exchange potential in satisfactorily fitting the large angle differential cross section data.

Since the WS potential failed to reproduce our data at angles larger than 130°, it was of interest to study whether the inclusion of Majorana exchange terms in both the real and the imaginary central potentials would provide a better description of the large angle data. To this end, an attempt was made with potentials of the form:

$$U_R(1+C_R P^r) f(r,r_R,a_R)$$

and

$$W_V(1+C_I P^r) f(r,r_I,a_I) ,$$

where U_R/W_V is the real/imaginary central potential strength, C_R/C_I the scaling factor for the real/imaginary exchange potential, and P^r the space exchange operator. Except for an enhancement of the back angle cross section beyond 150°, the calculations fail to provide any significant improvement over the standard Woods-Saxon fits.

3. Potential with wine bottle shape

For our energy range, microscopic theories[20] of the proton-nucleus potential have predicted a depression at the center of the real central potential due to increased nuclear density in this region, resulting in a wine bottle (WB) shape. It is not clear whether the origin of this WB shape is microscopic or related to relativistic treatments. In the analysis of the elastic scattering of 180 MeV protons from ^{56}Fe, Elton[21] found that the best fit real central potential had a WB shape. It was also found to reproduce large angle data of the elastic scattering of 200 MeV p+^{12}C.[8] Thus, we added a Gaussian term to the real central potential of the form:

$$\alpha \exp - \left[\frac{r}{\beta A^{1/3}} \right]^2 ,$$

where α and β are the WB parameters.

Compared to the fit using a simple WS potential, the WB potential reproduced the minimum at 97°, and the fit to the shoulder at $\sim 150°$ is also greatly improved. However, it incorrectly predicts a very deep minimum at 162°. Thus, it can be concluded that one obtains only very modest improvement at the largest angles.

The volume integral, J_R/A, and the rms radius $\langle R_R^2 \rangle^{1/2}$ of the real central potential are much smaller than those of the Woods-Saxon potential. While the two potentials are similar at the center, the simple Woods-Saxon potential is attractive for all values of r and the wine bottle potential becomes and stays repulsive for $r > 9$ fm. This very long, albeit small, repulsive tail is responsible for reducing both J_R/A and $\langle R_R^2 \rangle^{1/2}$.

4. Woods-Saxon squared (WS^2) potential

The OMP calculated from microscopic theories often has a shape quite different from a WS shape. For example, von Geramb *et al.*,[22] based on their calculations of the internucleon interaction in nuclear matter, found that the potential shape differs increasingly from WS as the bombarding energy increases.

In our analysis, the real WS^2 shape was chosen in another attempt to fit our large angle data. This choice was prompted by the slightly improved fit obtained with the WB potential which fell off more rapidly than the WS potential in the surface region. This is very similar to the behavior of a WS^2 potential.

The best fit WS^2 parameters from a ten-parameter search are shown in Table I and the fit to the data in Fig. 1 (dotted-dashed line). Up to $\sim 115°$, the WB and the WS^2 fits are not very different. Beyond that angle, the WS^2 seems to better reproduce the overall trend of the data.

A comparison of the WS^2 volume integral and rms radius with those of the WS potential shows a difference of about 3%. This small difference indeed confirms the gen-

eral belief that these two quantities can be rather unambiguously determined. On the other hand, the imaginary central potential strength is about 25% smaller, while the radius parameter is almost 10% larger. This is equivalent to a more transparent nucleus, but with a larger scattering surface.

D. Isotopic size comparison for ^{46,48,50}Ti

From Table I, it is clear that our results do not show any simple isotopic size dependence. The uncertainty of 7% in absolute normalization and 0.07° in the angle readings resulted in an error of about 1% in $\langle R^2\rangle_R^{1/2}$. If we assume a simple $A^{1/3}$ dependence, a change of two units in A would result in a change of $\sim 1\%$ in $\langle R^2\rangle_R^{1/2}$. We therefore, must expect the accuracy of any isotopic size comparison, based on our data, to be marred by the experimental error in the determination of $\langle R^2\rangle_R^{1/2}$.

From the folding model, we have

$$\langle R_R^2\rangle = \langle R_m^2\rangle + \langle r_d^2\rangle ,$$

where $\langle R_R^2\rangle$ is the mean square radius of the potential, and $\langle r_d^2\rangle$ the effective two-body interaction range. Using $\langle R_R^2\rangle^{1/2}=4.580$ fm (Table I) and $\langle R_m^2\rangle^{1/2}=3.55$ fm (based on Hartree-Fock calculations[23]) for ^{48}Ti, $\langle r_d^2\rangle$ was determined to be 8.37 ± 0.13 fm^2.

Then using this value of $\langle r_d\rangle$, the $\langle R_m^2\rangle$ for ^{46,50}Ti were obtained. Table II shows the results for the relative isotopic size extracted from our work. These are compared to similar results from proton scattering at 65 MeV,[7] alpha scattering at 140 MeV,[13] and electron scattering.[24,25]

It is clear that the proton data produce very similar results which are quite different from those of alpha scattering, and the different electron scattering experiments. The isotopic shift between ^{46}Ti and ^{48}Ti is about twice as large as that expected from an $A^{1/3}$ dependence; whereas the shift between ^{46}Ti and ^{50}Ti appears to be roughly following an $A^{1/3}$ dependence. We can naively offer a qualitative explanation for the negative sign of $(\langle R_m^2\rangle_{^{50}\mathrm{Ti}}^{1/2}-\langle R_m^2\rangle_{^{48}\mathrm{Ti}}^{1/2})$. In ^{50}Ti, the $1f_{7/2}$ neutron shell is completely filled and the neutrons are more tightly bound, resulting in a smaller size. However, we are still unable to explain the abnormally large shift in $\Delta\langle R_m^2\rangle^{1/2}$ between ^{46}Ti and ^{48}Ti extracted from our data.

E. Systematics of the OMP parameters

The best fit OMP parameters for all three Ti isotopes are presented in Table I. It is clear that the parameters for ^{48,50}Ti are very similar; the volume integrals and the rms radii of both real and imaginary potentials, and the calculated total reaction cross sections, differ by less than 1%. On the other hand, the parameters for ^{46}Ti do not seem to follow the same trend as those of ^{48,50}Ti. The volume integrals and the rms radii differ by $\sim 10\%$ from those of ^{48,50}Ti. It is not clear why the real spin-orbit strength of ^{46}Ti is about $\frac{1}{3}$ as large as those of ^{48,50}Ti.

One could speculate that this reduction in spin orbit is needed to reproduce the correct damping of the diffractive pattern of the data from $\sim 35°$ to 70°, which seems to be more pronounced in ^{46}Ti than in ^{48,50}Ti. It has been clearly demonstrated that the spin-orbit term is most sensitive to the data in this angular range, and that the destructive interference between the spin-flip and non-spin-flip scattering amplitudes results in the damping of the diffractive pattern.[6] Clearly, analyzing power data would be most helpful in resolving this problem.

F. Isospin dependence

With the Lane form the isospin dependence of the proton optical potential can be written as[26]

$$V_p = V_0 + V_1\left[\frac{N-Z}{A}\right] + \bar{V}_C ,$$

where V_1 is the strength of the symmetry potential. The potential $\bar{V}_C$ is the Coulomb correction term.

The symmetry potential has been studied in great detail by many authors. Patterson *et al.*[27] showed that $V_1 \simeq 17.7$ MeV for $25 < E_p < 45$ MeV over a wide range of nuclei. Jeukenne *et al.*[28] obtained the energy dependent form $V_1 \simeq 11.5 - 0.1E_p$ for proton energies up to 80 MeV. The relativistic calculation by Arnold and Clark[29] reported a complex symmetry potential, $\sim(18-i)$ MeV, for p+^{40}Ca at 26 MeV.

TABLE II. rms radii isotopic shift. ($\Delta\langle R^2\rangle^{1/2}$ is the change in $\langle R^2\rangle^{1/2}$ from isotope A to isotope B. m stands for matter distribution and c change distribution. All values are in 10^{-3} fm.)

	$\Delta\langle R^2\rangle^{1/2}$			$\Delta\langle R_m^2\rangle^{1/2}$				$\Delta\langle R_c^2\rangle^{1/2}$		
		65 MeV p	140 MeV α		65 MeV p	140 MeV α	Theor			Theor
$A-B$	a	b	c	a	b	c	d	e	f	d
48–46	85	38[e]	29	100±44	45	37±16	33	−15±10	3±15	2
50–48	−14	−24	32	−20±50	−45	40±16	32	−20±10	−16±15	3
50–46	71	14	61	90±62	0	78±16	65	−30±15	−13±15	5

[a]From this work.
[b]From Ref. 7.
[c]From Ref. 13.
[d]See Ref. 13.
[e]From Ref. 24.
[f]From Ref. 25.

TABLE III. Isospin dependence of the real equivalent potential, V_{EQ}, calculated from volume integrals.

Target	$\frac{N-Z}{A}$	J_R/A	V_{EQ} a	b	c
^{28}Si	0	243	21.40 (5.0)	22.02	21.94
^{46}Ti	0.0435	237	22.67 (4.4)	23.68	23.61
^{48}Ti	0.083	260	25.02 (4.0)	24.40	24.55
^{50}Ti	0.1200	259	25.07 (4.2)	25.06	25.40
^{58}Ni	0.0345	253	24.99 (2.0)	24.10	28.83
^{90}Zr	0.1111	256	27.22 (5.0)	26.48	26.37
^{120}Sn	0.1667	262	27.96 (3.4)	28.20	28.21
^{280}Pb	0.2115	276	30.67 (6.0)	31.06	30.78

[a] V_{EQ} calculated from the volume integrals. The number enclosed in the parentheses is the percentage error in V_{EQ}, based on that of the corresponding J_R/A.
[b] Using the relation $V_{EQ}=19.5+19.2(N-Z/A)+0.53Z/A^{1/3}$.
[c] Using the relation $V_{EQ}=20.1+24.3(N-Z/A)+0.4Z/A^{1/3}$.

The results of all available optical model analyses of 100 MeV data were used to extract the isospin dependence of the real central potentials. Because of the continuous ambiguities in the optical model parameters, instead of using the strengths determined in the analyses for V_p, it would be more consistent to use a V_{EQ} derived from the volume integrals. The volume integral can be written as

$$J_R/A \simeq \tfrac{4}{3}\pi r_0^3 V_{EQ}\left[1+\frac{\pi^2 a_0^2}{r_0^2 A^{2/3}}\right],$$

where r_0 and a_0 are determined by fitting the mean square radius, $\langle r_R^2\rangle$, with a linear dependence on $A^{2/3}$ and assuming

$$\langle r_R^2\rangle = \tfrac{3}{5}r_0^2 A^{2/3}+\tfrac{7}{5}\pi^2 a_0^2 .$$

The values obtained were $r_0=1.249$ and $a_0=0.755$. The values of V_{EQ} thus obtained are shown in Table III. For the Coulomb correction term the standard form commonly used in OM analyses was adopted,

$$V_C=0.4\frac{Z}{A^{1/3}} .$$

Figure 3 shows the quantity $V_{EQ}-0.4Z/A^{1/3}$ plotted as a function of $(N-Z)/A$. The symmetry potential derived from this curve is

$$V_1=24.3\pm2.3 \text{ MeV} .$$

More recently, based on microscopic calculations, Jeukenne *et al.*[28] suggested that V_C could have a larger value than is commonly assumed. Empirical support for a larger value is obtained from comparison of neutron and proton elastic scattering on $T=0$ nuclei at lower energy.[30] To explore this possibility a potential of the form

$$V_{EQ}=V_0+V_1\left[\frac{N-Z}{A}\right]+V_2\frac{Z}{A^{1/3}}$$

was adopted and V_1 and V_2 were treated as free parameters to be determined by the data. The result gave $V_1=19.2\pm4.2$ MeV and $V_2=0.53\pm0.09$ MeV as shown in Table III. This value of V_2 is consistent with the average value of 0.48 ± 0.1 obtained in Ref. 30. The fits are similar to those using 0.4 for the coefficient of the Coulomb correction term but the value of V_2 seems consistent with the predictions of Jeukenne *et al.* Using $V_C=1.38\beta Z/A^{1/3}$, one obtains $\beta=0.39\pm0.07$ for the linear energy dependence of the proton OM potential.

Giannini *et al.*[31] calculated the isospin dependence of the OM potential due to nonlocality. For 100 MeV protons, they obtained 21 MeV for the isoscalar term, 18.4 MeV for the symmetry potential, and a linear energy dependence of the proton potential with $\beta=0.36$. These values are in excellent agreement with the results of the present analysis.

G. Mean free path of 100 MeV protons

One interesting property of a particle propagating in nuclear matter is its mean free path (mfp). For protons at about 100 MeV, theoretical calculations typically yield a

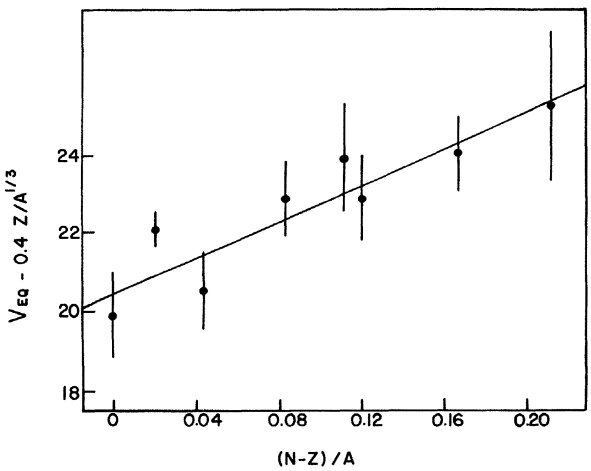

FIG. 3. Coulomb-corrected real potential plotted as a function of neutron excess, with $\bar{V}_C=0.4Z/A^{1/3}$.

mfp of about 3 fm,[32] whereas experimentally extracted values at the same energy are 5 fm or more.[6,33] Negele and Yazaki[34] have shown that this discrepancy can be resolved if the nonlocality of the OMP is treated properly. On the other hand, DeVries and DiGiacomo[35] question the relevance of the mfp concept for nucleons in finite nuclei, because of the variation in density at the surface.

We therefore decided to investigate whether the existing data at 100 MeV can provide some insight into the validity of extracting a mfp from elastic scattering data. The mfp, Λ, can be simply related to the imaginary part of the OMP by the expression[36]

$$\Lambda=\frac{\hbar}{2W_v}\left[\frac{2(E+U_R)}{M}\right]^{1/2}.$$

Table IV shows the values of Λ computed from the imaginary potential strength at 100 MeV from ^{28}Si to ^{208}Pb. The wide range of values obtained is a reflection of the large uncertainties inherent in the strength of the imaginary potential.

Alternatively, one can extract the mfp indirectly from the total reaction cross section, σ_R. Semiclassically, for a perfectly absorbing nucleus bombarded by protons, the reaction cross section can be written as

$$\sigma_R=\pi(R_0+\bar{\lambda})^2\left[1-\frac{U}{E}\right](1-T),$$

where $R_0=r_0A^{1/3}$ is the nuclear radius, $\bar{\lambda}$ is the de Broglie wavelength of the protons, $U=Zze^2/R_0$ is the Coulomb barrier height,

$$T=\frac{1-(1+2KR)e^{-2KR}}{2K^2R^2}$$

the nuclear transparency factor, $K=1/\Lambda$ is the reciprocal of the mfp, and $R=R_0+\bar{\lambda}$.

The best fit r_0 and K for the σ_R from OM calculations were found to be 1.43 fm and 0.194 fm^{-1}, respectively, corresponding to $\Lambda=5.2$ fm. The result is shown in Table V, where we compare the OM reaction cross sections with those calculated with the assumption that $\Lambda=5.2$ fm. The agreement between the two calculations is very good. The mfp obtained by this method agrees with that obtained by Nadasen *et al.*[6] ($\Lambda=5.2\pm1.0$ fm) and that obtained by Kirky and Link[15] ($\Lambda=5.6$ fm). However, the above equation, being sensitive to the value R_0, can lead to a rather small mfp if the value of R_0 is chosen to reproduce the reaction and total cross sections consistently.[37]

TABLE IV. The mfp (in fm) of 100 MeV protons as computed from best fit OM potentials.

	WS[a]	WS^2[b]
^{28}Si	8.13	
^{46}Ti	3.51	2.90
^{48}Ti	5.42[c]	5.09[c]
	(5.08)	(6.63)
^{50}Ti	5.18	4.82
^{58}Ni	7.02	
^{90}Zr	6.96	
^{120}Sn	6.92	
^{280}Pb	8.71	

[a]The form factors of both real and imaginary potentials have WS shapes.

[b]The form factor of the real potential has a WS^2 shape while that of the imaginary potential a WS shape.

[c]The first number is obtained from the best fit potential for the data range $9°\leq\theta\leq110°$ and that enclosed in parentheses for $9°\leq\theta\leq168°$.

TABLE V. Comparison of reaction cross sections in mb obtained from OM analysis with those determined using a mean free path of 5.2 fm.

	σ_R from OM calculations	$\sigma_R=\pi(R_0+\bar{\lambda})^2\left[1-\frac{U}{E}\right](1-T)$ $R_0=1.43\times A^{1/3}$, $K=0.194$
^{28}Si	441	468
^{46}Ti	663	664
^{48}Ti	696	686
^{50}Ti	701	707
^{58}Ni	771	779
^{90}Zr	1085	1058
^{120}Sn	1296	1289
^{208}Pb	1832	1839

H. Radial sensitivity of proton absorption

Because of the large uncertainties in the mean free paths derived from the imaginary potential strength, it was decided to investigate the radial region of the imaginary central potential to which the data are most sensitive. A "notch" perturbation with a depth of 15% of the imaginary potential and a width of 0.7 fm was introduced to the imaginary potential, and the resulting χ^2 per point as a function of the radial location of the notch was observed.

Figure 4 shows the change in χ^2/χ_0^2 as the centroid of the notch perturbation is moved radially, where χ_0 is obtained from the unperturbed fit. The arrows, labeled R_a and R_b, are the radii at which the real and imaginary potentials, respectively, reach one-half their central value. It is clear that even at 100 MeV, the incident protons do not penetrate very deeply into the nucleus before being absorbed. The data seem to be very insensitive to changes in the central region of the imaginary potential. This ambiguity in the imaginary potential is a reflection of the inherent uncertainty in determining the scattering amplitudes from the data. This might be the reason for the large uncertainties in the derived mean free paths.

It is interesting to observe that when the notch is near the center, the resulting fit to the data resembles that of the unperturbed potential. As the notch moves towards the surface, a backward peak begins to emerge in the predicted elastic scattering cross section at $\sim160°$. This peak is more representative of the data, suggesting the necessity of a different and perhaps slightly more complicated parametrization of the imaginary potential, particularly near the surface, in order to be able to reproduce the large angle data.

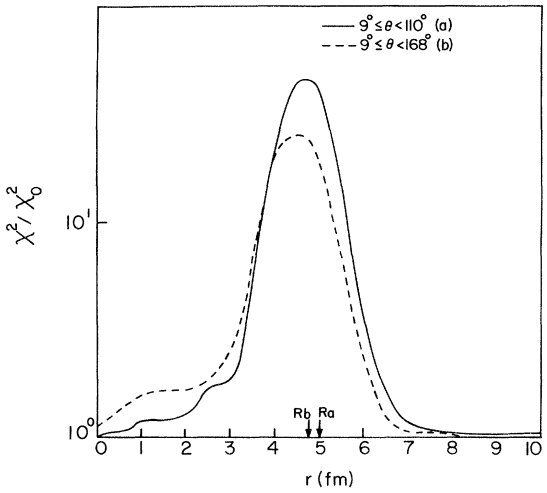

FIG. 4. Radial sensitivity of the ^{48}Ti elastic scattering data to the central imaginary potential.

V. ANALYSIS OF THE INELASTIC SCATTERING CROSS SECTIONS

A simple analysis of the inelastic scattering differential cross sections for the excitation of the first excited (2^+) states was carried out with both the distorted wave Born approximation (DWBA) and the coupled channels Born approximation (CCBA) based on a collective model description of these states. The computer codes used were DWUCK4, CHUCK, and ECIS. In first order the expansion of the target deformation about a spherical OMP for states described by either a small, one-phonon vibrational or an axially symmetric rotational model, lead to rather similar calculated cross sections.[38] We therefore used the standard derivative form for the coupling term:

$$\frac{d}{dr}[\beta_R R_R V(r)+i\beta_I R_I W(r)] ,$$

where $\beta_{R,I}$ is the quadrupole deformation parameter and $V(r)/W(r)$ is the real/imaginary OM potential with half radius R_R/R_I. It is sometimes customary to include a Coulomb excitation term, but preliminary calculations indicated that it had a negligible effect. Hodgson made similar observations.[39]

In the DWBA, assuming the deformation parameters $\beta_R=\beta_I=\beta_2$, the predicted inelastic cross section is directly proportional to the square of the coupling coefficient. Thus, by comparing data with calculations one can extract β_2. The values we obtained are shown in Table VI together with previous results. Except for the results from 35.2 MeV proton scattering,[40] the values of β_2 extracted from the proton or alpha inelastic scattering experiments agree quite well.

Figure 2 shows the results of DWBA calculations for all three targets. The solid curves scale as $(\beta_2)^2$. Also shown as dashed curves is an alternative mixture of real and imaginary form factors in which $(\beta_R R_R)=(\beta_I R_I)=(\beta_2 R)$. Both curves fail to reproduce the data satisfactorily, predicting too deep minima. This might be attributed to the lack of a deformed spin-orbit term in the collective form factor. The oscillations in the data are strongly damped in the range of 40°–70°. This is indeed the region which is most sensitive to the spin-orbit term.

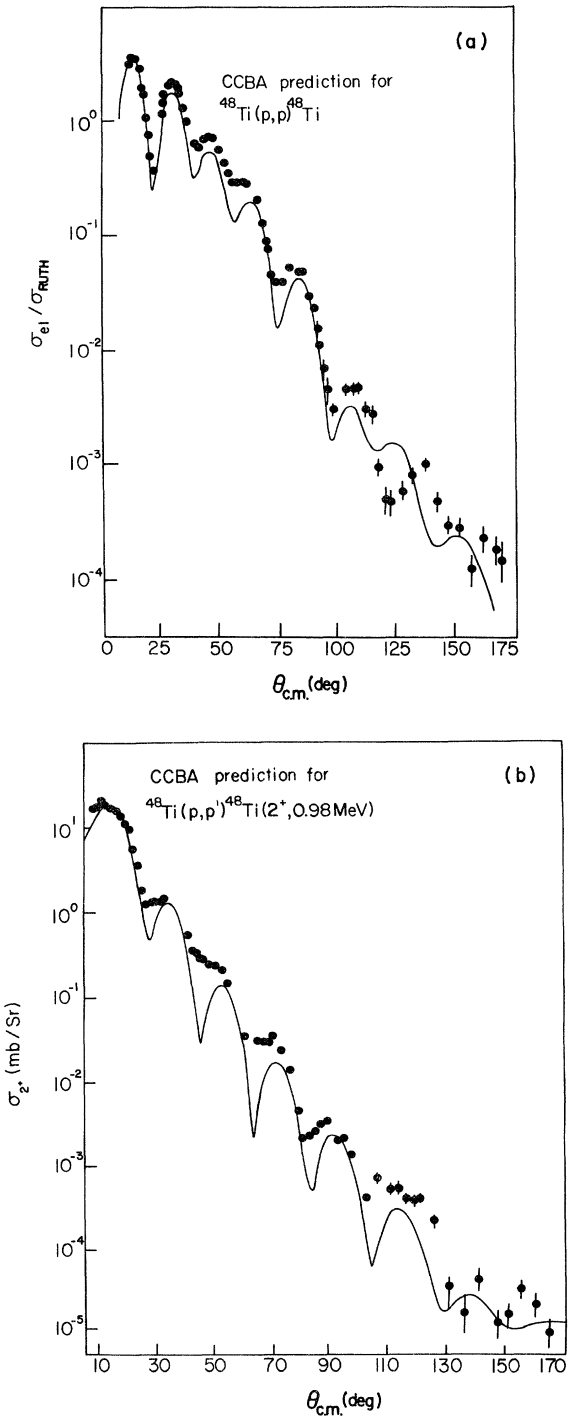

FIG. 5. (a) Comparison of CCBA predictions with the elastic scattering data of ^{48}Ti. (b) Comparison of CCBA predictions with the differential cross section for the first 2^+ state of ^{48}Ti.

We also carried out coupled channels calculations with the values of β_2 extracted from the DWBA calculations. Figure 5 shows the CCBA results for ^{48}Ti. The CCBA underestimates σ_{2+} by about 25%, and does not reproduce the shape any better than the DWBA [Fig. 5(b)]. Howev-

TABLE VI. Comparison of β_2.

	Present work	Coulomb excitation[a]	114.4 MeV p[b]	35.2 MeV p[c]	43 MeV α[d]
^{46}Ti	0.24	0.29	0.25	0.28	0.23
^{48}Ti	0.20	0.265	0.22	0.25	0.19
^{50}Ti	0.14	0.175	0.14	0.19	0.136

[a]From Reference 41. β_2 was computed from the corresponding $B(E_2)$ value, measured in Coulomb excitation experiment, and $R=1.2A^{1/3}$.
[b]Reference 42.
[c]Reference 40.
[d]Reference 43.

er, it seems to give a fairly accurate prediction of the cross section at such large angles, whereas DWBA predictions are about one order of magnitude too large. It is noted that the trend and magnitude of the elastic scattering data beyond 150° is perhaps better reproduced by the CCBA than the OM analysis [Fig. 5(a)]. No attempt was made to refit the elastic scattering data with the CCBA analysis. However, the present calculations suggest the importance of coupled channels effects, particularly at large angles. This might explain the difficulties encountered by conventional OM analyses to reproduce elastic scattering data at large angles.

VI. SUMMARY AND CONCLUSION

We have made precise measurements of the differential cross sections for the elastic and inelastic scattering to the first excited 2^+ states of 101.3 MeV protons from ^{46,48,50}Ti. The angular range covered was from 9° to 110° for ^{46,50}Ti and 9° to 168° for ^{48}Ti. The overall uncertainty in absolute cross section is about 7%, arising mainly from target thickness uncertainties and to a lesser extent, the reaction tail correction of the Ge detectors.

The elastic scattering data were analyzed with a local optical model potential (OMP). For isotopic comparisons with ^{46,50}Ti, only the 9°–110° data of ^{48}Ti was used. Very good fits were obtained for all three isotopes. The best fit parameters for ^{46}Ti show some deviations from those of ^{48,50}Ti. The uncertainty in the best fit parameters due mainly to the uncertainty in the absolute normalization has rendered any relative isotopic size comparison unreliable.

Combining all the 100 MeV proton data (^{46,48,50}Ti, ^{58}Ni, ^{90}Zr, ^{120}Sn, and ^{208}Pb), we determined the isospin component of the real potential, using the conventional $0.4Z/A^{1/3}$ form for the Coulomb correction term, to be 24.3 ± 2.3 MeV. Following the work of Jeukenne *et al.*,[28] we also attempted to extract the isospin potential by treating the coefficient of the Coulomb correction term as a free parameter and obtained a value of 19.2 ± 4.2 MeV. Our results are in excellent agreement with the theoretical calculations of Giannini *et al.*[31]

By introducing a localized perturbation into the OMP, we found that the data are quite insensitive to the imaginary potential at small radii. This is in agreement with the results of earlier investigations.[44] The consequence of this is that the mean free path (mfp) determined from the imaginary potential strength could have large uncertainties.

Using an expression which relates the total reaction cross section to that of an absorbing sphere and takes explicitly into consideration the Coulomb repulsion between the target and the projectile, and the transparency of the target at higher incident energies, we obtained a mfp of 5.2 fm. More realistically, one expects the mfp to be A dependent, especially for the light nuclei, and become almost constant for very heavy targets which approach the limit of infinite nuclear matter.[45]

We were unable to obtain any high quality fits to the large angle data of ^{48}Ti. The conventional Woods-Saxon (WS) real form factor fails to reproduce the data at large angles satisfactorily. In spite of the successes of other works at different energies,[19] incorporation of an exchange term of the simple Majorana form into our OMP did not provide any significant improvement. We also found no evidence that our data prefers a real potential with a slightly less attractive center, as indicated by analyses of elastic scattering data at 155,[46] 180,[20,47] and 200 MeV,[8] perhaps due to our lower incident proton energy. On the other hand, the data seem to favor a sharper falloff at the surface of the real potential, such as that provided by the Woods-Saxon squared (WS^2) form. Contrary to the results of Nadasen *et al.*,[6] we found the WS^2 real potential form to provide an improved fit to our data, particularly in predicting the general trend of the cross section at large angles.

The inelastic scattering data were analyzed with DWBA and CCBA calculations. We assumed collective excitation of the target, characterized by the deformation parameters, β. The β values obtained were in satisfactory agreement with electromagnetic or other inelastic scattering measurements.

The inelastic scattering data of ^{48}Ti demonstrated clearly the inadequacy of the DWBA, particularly at large angles where the prediction is almost ten times too large. On the other hand, the CCBA provides better agreement with the inelastic scattering data and predicts the very large angle elastic scattering data fairly well, possibly better than the OM analysis. This suggests the importance of couple-channels effects at large momentum transfers.

Recent studies[48] have suggested that the coupling between the ground state and the high-lying states in the giant multipole resonance region is important for large angle elastic and inelastic scattering, and this coupling manifests itself as an effective l-dependent absorptive and repulsive OMP. Such coupling might provide more insight into the understanding of large angle elastic and inelastic scattering data.

In spite of the high quality of our data, we believe more precise measurements, particularly of the absolute normalization, are essential for the studying of such small effects as relative isotopic size and isospin dependence. Polarization measurements are necessary if the spin-orbit potential is to be better determined. Finally, large angle data are important for the study of coupled-channels effects.

ACKNOWLEDGMENTS

The authors are grateful to the University of Maryland Computer Science Center for its generous allocation of computer time. This work was supported in part by the National Science Foundation.

*Present address: Indiana University Cyclotron Facility, Bloomington, IN 47405.

†Present address: National Bureau of Standards, Washington, D.C. 20234.

‡Present address: University of Michigan—Dearborn, 4901 Evergreen Road, Dearborn, MI 48128.

[1]H. Feshbach, C. E. Porter, and V. F. Weisskopf, Phys. Rev. 96, 448 (1954).

[2]F. G. J. Perey, Phys. Rev. 131, 745 (1963); F. G. J. Perey and B. Buck, Nucl. Phys. 32, 353 (1962).

[3]F. Becchetti and G. W. Greenlees, Phys. Rev. 182, 1190 (1969).

[4]W. T. H. Van Oers and J. M. Cameron, Phys. Rev. 184, 1061 (1969); W. T. H. Van Oers and H. Haw, Phys. Lett. 45B, 227 (1973).

[5]K. Kwiatkowski and N. S. Wall, Nucl. Phys. A301, 349 (1978).

[6]A. Nadasen *et al.*, Phys. Rev. C 23, 1023 (1981).

[7]H. Sakaguchi *et al.*, Research Center for Nuclear Physics Annual Report, 1978, p. 12.

[8]H. O. Meyer, P. Schwandt, G. L. Moake, and P. P. Singh, Phys. Rev. C 23, 616 (1981).

[9]C. P. Dover and Nguyen Van Giai, Nucl. Phys. A177, 559 (1971); A190, 373 (1972); R. W. Manweiler, *ibid.* A240, 373 (1975); B. Sinha, Phys. Rep. 20C, 1 (1975).

[10]L. G. Arnold *et al.*, Phys. Rev. C 14, 1878 (1976); L. G. Arnold, B. C. Clark, and R. L. Mercer, *ibid.* 19, 917 (1979).

[11]J.-P. Jeukenne, A. Lejeune, and C. Mahaux, Phys. Rep. 25C, 83 (1976); Phys. Rev. C 15, 10 (1977); 16, 80 (1977).

[12]F. A. Brieva and J. R. Rook, Nucl. Phys. A291, 299 (1977); A291, 317 (1977); A297, 206 (1978).

[13]P. L. Roberson *et al.*, Phys. Rev. Lett. 42, 54 (1979).

[14]M. A. Melkanoff *et al.*, in *Methods in Computational Physics,* edited by B. Alder, S. Fernbach, and M. Ropenberg (Academic, New York, 1966), Vol. 6, p. 1.

[15]P. Kirky and W. T. Link, Can. J. Phys. 44, 1847 (1966).

[16]A. Ingermarsson and G. Tibell, Phys. Scr. 4, 235 (1971).

[17]F. Coester and H. Kummel, Nucl. Phys. 9, 225 (1958); H. Rollnik, Z. Naturforsch. 13a, 59 (1958).

[18]G. W. Greenlees, W. Makofske, Y. C. Tang, and D. R. Thompson, Phys. Rev. C 6, 2057 (1972).

[19]D. R. Thompson, Y. C. Tang, and R. E. Brown, Phys. Rev. C 5, 1939 (1972); L. G. Votta, P. G. Roos, N. S. Chant, and R. Woody, III, *ibid.* 10, 520 (1974); N. P. Goldstein, A. Held, and D. G. Stairs, Can. J. Phys. 48, 2629 (1970); V. Comparat *et al.*, Phys. Rev. C 12, 251 (1975).

[20]W. Banhoff, H. V. Geramb, and G. Palla, Hungarian Academy of Sciences Report No. KFKI-1980, 1980, p. 123; see also *Proceedings of the Conference on Microscopic Optical Potentials, Hamburg, 1978,* edited by H. V. von Geramb (Springer, Berlin, 1979).

[21]L. R. B. Elton, Nucl. Phys. 89, 69 (1966).

[22]H. V. von Geramb, F. A. Brieva, and J. R. Rook, in *Proceedings of the Conference on Microscopic Optical Potentials, Hamburg, 1978,* edited by H. V. von Geramb (Springer, Berlin, 1979).

[23]J. W. Negele and D. Vautherin, Phys. Rev. C 5, 1472 (1972).

[24]E. F. Romberg *et al.*, Nucl. Phys. A173, 124 (1971).

[25]J. Heisenberg *et al.*, Phys. Rev. C 6, 381 (1972).

[26]A. M. Lane, Nucl. Phys. 35, 676 (1962); G. R. Satchler, in *Isospin in Nuclear Physics,* edited by D. H. Wilkinson (North-Holland, Amsterdam, 1969).

[27]D. M. Patterson, R. R. Doering, and A. Galonsky, Nucl. Phys. A263, 261 (1976).

[28]J.-P. Jeukenne, A. Lejeune, and C. Mahaux, Phys. Rev. C 15, 10 (1977).

[29]L. G. Arnold and B. C. Clark, Phys. Rev. C 23, 15 (1981).

[30]J. Rapaport, Phys. Rep. 87, 25 (1982); J. Rapaport *et al.*, Nucl. Phys. A286, 232 (1977).

[31]M. M. Giannini, G. Ricco, and A. Zucchiatai, in *Proceedings of the Conference on Microscopic Optical Potentials, Hamburg, 1978,* edited by H. V. von Geramb (Springer, Berlin, 1979).

[32]K. Kikuchi and M. Kawai, *Nuclear Matter and Nuclear Reactions* (North-Holland, Amsterdam, 1968), Chap. 2; M. T. Collins and J. J. Griffin, Nucl. Phys. A348, 63 (1980).

[33]A. Bohr and B. Mottelson, *Nuclear Structure* (Benjamin, New York, 1969); J. P. Schiffer, Nucl. Phys. A335, 348 (1980).

[34]J. W. Negele and K. Yazaki, Phys. Rev. Lett. 47, 71 (1981).

[35]R. M. DeVries and N. J. DiGiacomo, Los Alamos National Laboratory Report LA-UR-80-2736, 1980.

[36]L. R. B. Elton, *Introductory Nuclear Theory* (Saunders, Philadelphia, 1966), p. 174.

[37]R. Dymrz and T. Kohmura, Phys. Lett. 124B, 446 (1983).

[38]O. Karban *et al.*, Nucl. Phys. A147, 461 (1970).

[39]P. E. Hodgson, *Nuclear Reactions and Nuclear Structure* (Clarendon, Oxford, 1971), p. 405.

[40]E. Fabrici *et al.*, Phys. Rev. C 21, 844 (1980).

[41]P. H. Stelson and L. Grodzins, Nucl. Data, Sect. A 1, 21 (1965).

[42]H. F. Lutz, W. Bartolini, T. H. Curtis, and G. M. Klody, Phys. Rev. 187, 1479 (1969).

[43]J. L. Yntema and G. R. Satchler, Phys. Rev. 161, 1137 (1967).

[44]J. G. Cramer and R. M. DeVries, Phys. Rev. C 22, 91 (1980); G. R. Satchler, in *Proceedings of the International Conference on Reactions Between Complex Nuclei, Nashville, Tennessee, 1974,* edited by R. J. Robinson *et al.* (North-Holland, Amsterdam, 1974), p. 171; P. J. Moffa, C. B. Dover, and J. P. Varey, Phys. Rev. C 13, 147 (1976).

[45]R. C. Johnson (private communication).

[46]I. Brissaud, Z. Phys. A 300, 247 (1981).

[47]M. Jaminon, C. Mahaux, and P. Rochus, Nucl. Phys. A365, 371 (1981).

[48]J. Weise, Z. Phys. A 300, 329 (1981).